High-Affinity Chelator Thiols for Switchable and Oriented Immobilization of Histidine-Tagged Proteins: A Generic Platform for Protein Chip Technologies

Ali Tinazli,[a] Jilin Tang,[a] Ramûnas Valiokas,[a, c] Srdjan Picuric,[a] Suman Lata,[a] Jacob Piehler,[a] Bo Liedberg,[b] and Robert Tampé*[a]

Abstract: Protein micro-/nanoarrays are becoming increasingly important in systematic approaches for the exploration of protein–protein interactions and dynamic protein networks, so there is a high demand for specific, generic, stable, uniform, and locally addressable protein immobilization on solid supports. Here we present multivalent metal-chelating thiols that are suitable for stable binding of histidine-tagged proteins on biocompatible self-assembled monolayers (SAMs). The architectures and physicochemical properties of these SAMs have been probed by various surface-sensitive techniques such as contact angle goniometry, ellipsometry, and infrared reflection–absorption spectroscopy. The specific molecular organization of proteins and protein complexes was demonstrated by surface plasmon resonance, confocal laser scanning, and atomic force microscopy. In contrast to the mono-NTA/His$_6$ tag interaction, which has major drawbacks because of its low affinity and fast dissociation, drastically improved stability of protein binding by these multivalent chelator surfaces was observed. The immobilized histidine-tagged proteins are uniformly oriented and retain their function. At the same time, proteins can be removed from the chip surface under mild conditions (switchability). This new platform for switchable and oriented immobilization should assist proteome-wide wide analyses of protein–protein interactions as well as structural and single-molecule studies.

Keywords: biosensors · molecular recognition · protein arrays · protein engineering · self-assembled monolayers · single molecule studies · surface analysis

Introduction

Protein arrays and biosensors are playing increasingly important roles in the postgenomic era for study of protein function and mapping of protein interaction networks.[1–8]

Solid-phase-based assays are becoming more and more important in functional proteomics and medical diagnostics. These solid-phase techniques require the immobilization of proteins in their native states. Most importantly, protein function should not be distressed by the immobilization. Functional and structural studies often require uniformly oriented immobilization of proteins. Physisorption is usually unspecific and can result in protein unfolding and inactivation. Covalent binding of the protein to a reactive surface through surface-accessible residues often lacks regiospecificity and hence correct orientation of the immobilized protein. Additionally, the reactive site of a protein can be blocked by the immobilization procedure, resulting in reduced activity of the protein.[9]

To circumvent these problems, surface capture agents, modified with a tag for specific interaction with the surface, can be used to immobilize proteins. This strategy is based on the established capture agent/fusion protein pairs that have been developed for purification in affinity chromatography. Many fusion proteins with popular tags—such as glu-

[a] Dipl.-Biochem. A. Tinazli, Dr. J. Tang, Dr. R. Valiokas, S. Picuric, S. Lata, Dr. J. Piehler, Prof. Dr. R. Tampé
Institute of Biochemistry, Biocenter
Johann Wolfgang Goethe-University
Marie-Curie-Strasse 9, 60439 Frankfurt (Germany)
Fax: (+49) 69-798-29495
E-mail: tampe@em.uni-frankfurt.de

[b] Prof. Dr. B. Liedberg
Sensor Science and Molecular Physics Division
Dept. of Physics and Measurement Technology
Linköping University, 581 83 Linköping (Sweden)

[c] Dr. R. Valiokas
Present address: Molecular compounds physics laboratory
Institute of Physics, Savanoriu 231, 02300 Vilnius (Lithuania)

Supporting information for this article is available on the WWW under http://www.chemeurj.org/ or from the authors.

tathione S-transferase,[10–12] maltose-binding protein,[13,14] the FLAG peptide,[15,16] and the well known oligohistidine[17–20]—are available, whilst other techniques for selective and covalent immobilization of fusion proteins have been reported recently.[21–23] These approaches have the common feature that the protein of interest is fused to a protein trapped irreversibly by its pseudosubstrate (suicide substrate) on the chip surface.

Over the last decade, the N-nitrilotriacetic acid (NTA)/ His$_6$-tag chelator system[24] has become a powerful and universal tool for the one-step isolation and purification of gene products.[20,25] The small and flexible tag allows the function of the protein to be preserved. Additionally, the binding is reversible, with dissociation inducible at low pH or by addition of imidazole or EDTA. While such affinity capturing is suitable for protein purification, applications requiring long-term stability on geometrically defined surfaces such as protein arrays and biosensors have been compromised by problems with metal leaching and rapid protein dissociation.[26,27] The chelator lipid concept with NTA-functionalized lipids[28,29] gave insights into functional aspects of immobilized proteins.[30–32] Evidence for multivalent interactions between the His$_6$ tag and the NTA groups was found in experiments involving immobilization of His$_6$-tagged proteins on chelating lipid membranes with chelators at different surface concentrations.[30,31] It was concluded that stable binding of His$_6$-tagged proteins takes place at a specific surface concentration threshold value of NTA lipid. Cumulated NTA clusters with multivalent interaction sites to His$_6$ tags may thus overcome the limitation of protein dissociation in the conventional NTA/His$_6$ tag interaction.

An ideal protein chip possesses docking sites that interact stably, specifically, and stoichiometrically (1:1) with proteins. The immobilized proteins should be uniformly oriented, preserving their function. Furthermore, proteins should be detachable under mild conditions, allowing further analyses and regeneration of the chip. Here we present surfaces with switchable multivalent chelators for stable, specific, functional, and reversible immobilization of His$_6$-tagged proteins. We have combined the stability, robustness, and broad range of application of self-assembled monolayers (SAMs) on gold[33–36] with these novel multivalent metal-chelating thiols. Surface and protein binding properties of multi- and monovalent chelator thiols mixed with various ratios of a protein-repellent matrix thiol[34,37,38] were investigated. The application of different proteins in surface plasmon resonance (SPR), fluorescence microscopy, and atomic force microscopy (AFM) experiments demonstrated—in contrast with the conventional NTA/His$_6$ tag interaction—stable and switchable binding of the immobilized protein on the chelating surfaces.

Results and Discussion

Synthesis of mono- and multivalent chelator thiols: Surfaces of gold allow more flexible and convenient chemical, almost defect-free, modification than their silicon (oxide) counterparts in the formation of self-assembled monolayers (SAMs). The antiadsorptive properties of oligoethylene glycol (OEG) thiols have been optimized to minimize unspecific protein adsorption.[34–38] The triethylene glycol matrix thiol **6** (Scheme 1) operates as a protein-repellent matrix that can be doped with functionalized thiols to form a mixed SAM. In addition to the mono-NTA thiol **9**, we also introduced a multivalent chelator thiol **12** (bis-NTA thiol) for stable and switchable immobilization of histidine-tagged proteins.

The synthesis of all the thiols is modular and based on 16-mercaptohexadecanoic acid linked to a triethylene glycol (EG$_3$) moiety. The question of the optimal alkyl chain length, which determines the chemisorption rate on gold and thus SAM formation, is still controversial,[39] but for our synthesis we chose a hexadecane alkyl unit. The synthesis was optimized so that a single precursor **3** would enable easy and economic assembly of different compounds, such as the matrix thiol **6**, the mono-NTA thiol **9**, and the bis-NTA thiol **12**, as outlined in Scheme 1. The thiol group in the initial compound 16-mercaptohexadecanoic acid (**1**) was protected by treatment with zinc acetate to yield 16-acetyl-sulfanyl-hexadecanoic acid (**2**). This intermediate was coupled to the triethylene glycol (EG$_3$) moiety through an ester bond to afford the precursor **3**. Matrix thiol **6** was synthesized from the precursor **3** by deprotection of the sulfur group with hydrazinium acetate. Coupling of *tert*-butyl-protected mono-NTA **4** or bis-NTA **5** through carbamate linkages and subsequent deprotection of the thiol and carboxyl groups yielded mono-NTA thiol **9** and bis-NTA thiol **12**, respectively.

The deprotection strategy was a critical aspect of the synthesis. At first the thiol groups in **7** and **10** were deprotected with hydrazinium acetate to yield **8** and **11**. Because of the possibility that free thiol groups might become butylated by the liberated *tert*-butyl moieties from the deprotected NTA groups an efficient strategy for capturing of these *tert*-butyl groups was needed. Deprotection of the thioether bond might require harsh reaction conditions and probably degrade the intermediates and thus lower the yields of the final products. Trifluoroacetic acid (TFA) was therefore used for deprotection and ethanedithiol (EDT) as a scavenger for the released *tert*-butyl groups, yielding the final products **9** and **12**. In contrast to other described functionalized thiols, the metal-chelating group was coupled by ester—rather than by ether or amide—chemistry, giving higher efficiency and highly flexible synthesis. The final products (**6**, **9**, **12**) were analyzed by mass spectrometry for their long-term stability in solution and within self-assembled monolayers; no hydrolysis of the ester bond was observed even after five days. Details on the synthesis and analyses of all products are given in the Supporting Information.

Formation of self-assembled monolayers with multivalent chelator thiols: SAMs formed from one-component solu-
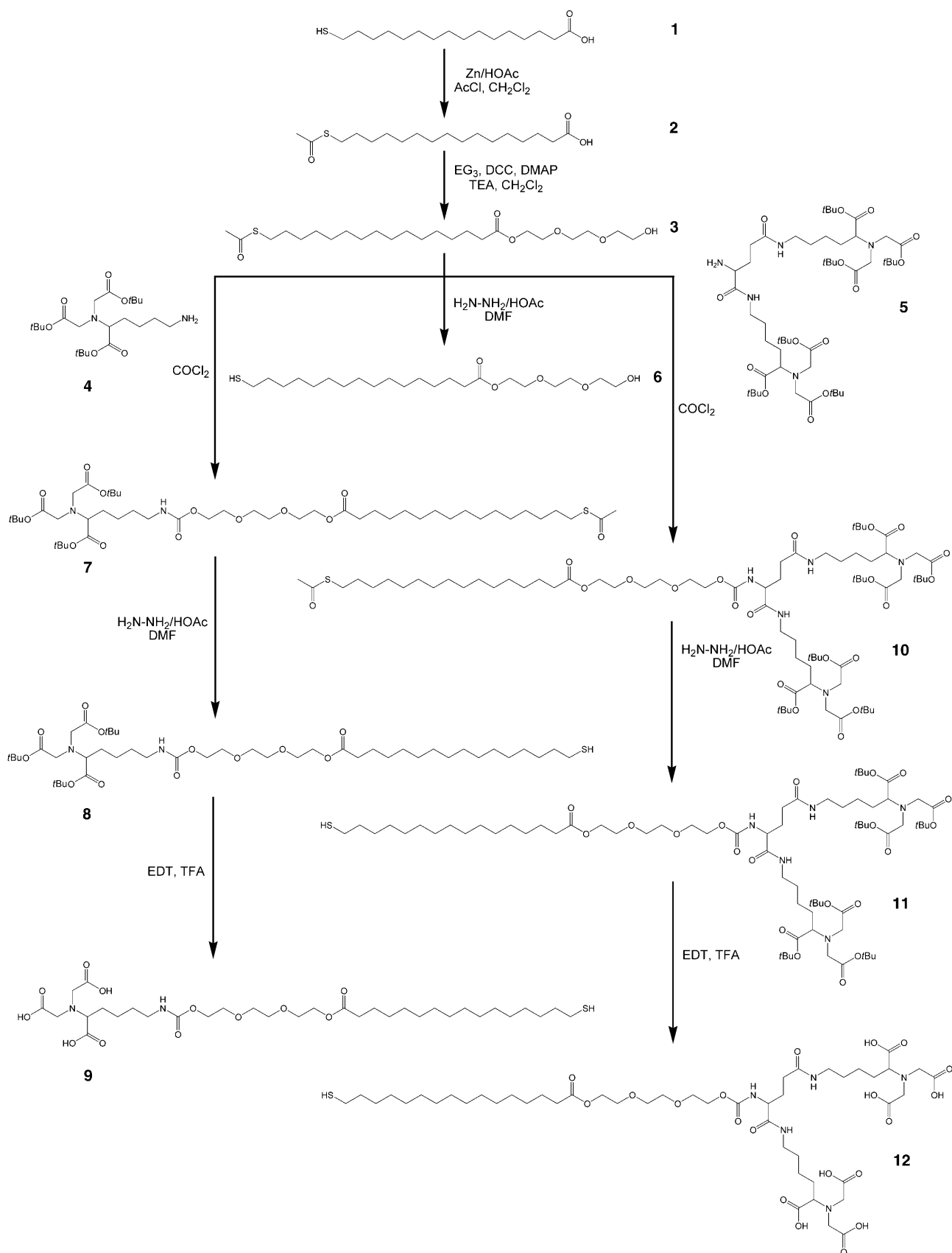
Scheme 1. Modular synthesis of mono- and multivalent chelator thiols (**9** and **12**).

tions of matrix thiol **6**, mono-NTA thiol **9**, or multivalent bis-NTA thiol **12** in acetonitrile (hereafter referred as SAM **6**, SAM **9**, and SAM **12**, respectively) were analyzed by contact angle goniometry and ellipsometry (Figure 1).
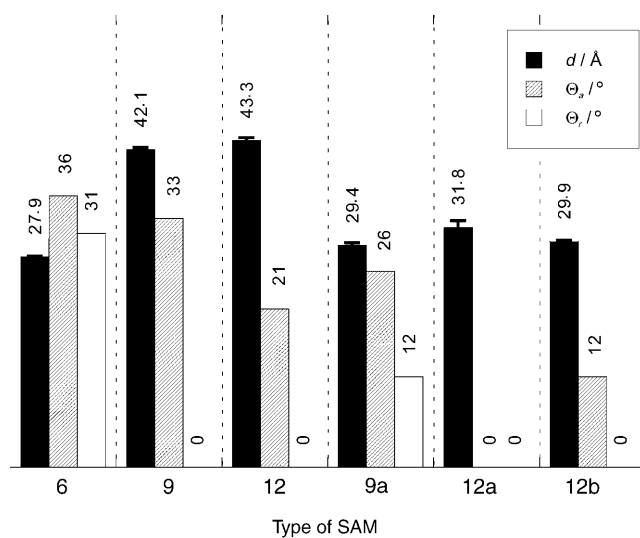

Figure 1. Ellipsometric thickness (d) and water contact angles (advancing θ_a and receding θ_r) of the investigated self-assembled monolayers (SAMs). Compounds **6**, **9**, and **12** were used to form SAMs **6**, **9**, and **12**, respectively. Mixed SAMs **9a**, **12a**, and **12b** were formed from mixtures of compound **9** (3 mol%) and **6** (**9a**), or **12** (3 mol%) and **6** (**12a** and **12b**). Acetonitrile was used as a solvent for all the SAMs except for **12b**, which was formed in THF. The value "0" is used to denote contact angles $<10°$.

The contact angles of SAM **6** indicate that the alkyl portion of the molecules is attached to gold, and that the triethylene glycol (EG$_3$)[40] and NTA portions are exposed to the ambient. The thickness (d) of SAM **6** suggests that the all-*trans* alkyl chains are tilted at approximately 30° to the surface normal, corresponding to a theoretical alkyl layer thickness of around 18 Å. Since the average incremental thickness per EG unit is 3 Å,[41,42] the total expected d for SAM **6** would be 27 Å, a value in good agreement with the experimental results. SAMs **9** and **12** display θ_a values that significantly differ from SAMs terminated by carboxy groups (typically below 10°[43]). The contact angle hysteresis is also large, suggesting that the surface is heterogeneous (that is, the pure mono-NTA and bis-NTA SAMs appear to be disordered).

Infrared reflection–absorption spectroscopy (IRAS) was used to provide information about the molecular packing and the orientations of different groups in the SAMs under investigation. The CH stretching region indicates that SAM **6** consists of a layer of densely packed, crystalline alkyl chains, as evidenced by the asymmetric (ν_a) and symmetric (ν_s) CH$_2$ stretches of the alkyl chains at 2918 and 2850 cm^{-1}, respectively (Figure 2a). The CH$_2$ ν_a and ν_s modes appear as a shoulder near 2950 cm^{-1} and as broad features between the sharp alkyl peaks originating from the ethylene glycol tails. A distinctive ν_a peak close to 2890 cm^{-1} is indicative of ethylene glycol tails adopting the helical con-

formation. The absence of this peak suggests that the EG$_3$ tails do not adopt a helical conformation. Instead they more likely adopt an amorphous-like conformation.[44,45] The low-frequency region of SAM **6** (Figure 2b), which is nearly identical to that of the previously reported EG$_4$-terminated SAM,[40,44] contains the ester ν(C=O) mode at 1740 cm^{-1} and the CH$_2$ scissors modes at 1468/1455 cm^{-1},[40,46] together with other ester and EG$_3$ related peaks below 1300 cm^{-1} (not shown). For SAM **9**, the alkyl ν_a(CH$_2$) peak is broadened and shifted upwards to 2920 cm^{-1}, a consequence of an increasing population of *gauche* defects. Moreover, for SAM **12**, the ν_a and ν_s modes appear at 2925 and 2856 cm^{-1}, respectively, indicating liquid-like alkyl chains (that is, the alkyl layer seems to collapse due to the space-demanding bis-NTA group). The specific IR signature of the tethered NTA groups[47,48] can be found in the fingerprint region (Figure 2b). First of all, a strong carboxyl ν(C=O) peak is found at 1723 cm^{-1}.[49] Second, significant proportions of the terminal carboxylic groups are deprotonated, as evidenced by strong peaks at 1672 cm^{-1} (1662 cm^{-1} for **12**) and 1404 cm^{-1} due to carboxyl ν_a and ν_s modes, respectively. The amide II band at 1542 cm^{-1} can also be found in the fingerprint region, while the amide I band overlaps with the much stronger carboxyl ν_a peak discussed above.

From the above findings it is clear that, for specific protein immobilization through the His$_6$ tag, the chelator groups should be dispersed in an inert two-dimensional "matrix" provided by **6**. In the previous studies on His$_6$-tag protein immobilization on planar lipid bilayers, 3 mol% concentrations of NTA-lipids gave good results.[26] Details on the mixing behavior and on how different mixing ratios and solvents affect the structure and surface concentration in mixed SAMs of **6**, **9**, and **12** are to be published elsewhere (manuscript in preparation). Because of their superb properties we discuss here only SAMs formed from 3 mol% mixtures of **9** or **12** with **6** in acetonitrile and THF, which provided an optimal platform for the specific immobilization of histidine-tagged proteins.

Mixed SAMs **9a** and **12a** formed from acetonitrile solutions of either **9** or **12** (3 mol%) and **6** (97 mol%) are thicker than SAM **6** (Figure 1). They have smaller contact angles with higher hysteresis than SAM **6**, but most importantly the hysteresis—and thereby the heterogeneity—is less than in the single-component SAMs of **9** and **12**. Moreover, the stable position of the alkyl ν_a and ν_s peaks confirm that the alkyl chains are densely packed in a crystalline, all-*trans* conformation (Figure 2a). The terminal NTA groups can be easily recognized in the fingerprint region: the ν_a(COO$^-$) peak appears at 1677 and 1664 cm^{-1} for **9a** and **12a**, respectively. If a similar random orientation of the NTA groups in SAMs **9a** and **12a** is assumed, the diagnostic NTA peaks can be used to compare the fraction of NTA moieties in the SAMs. For this purpose, the ester ν(C=O) peak is subtracted from the spectra of the mixed SAMs, and the remaining peaks are integrated in the region from 1745 to 1577 cm^{-1}. The integrated peak intensities indicate that the total amount of NTA in SAM **12a** is 3.3 times higher than in
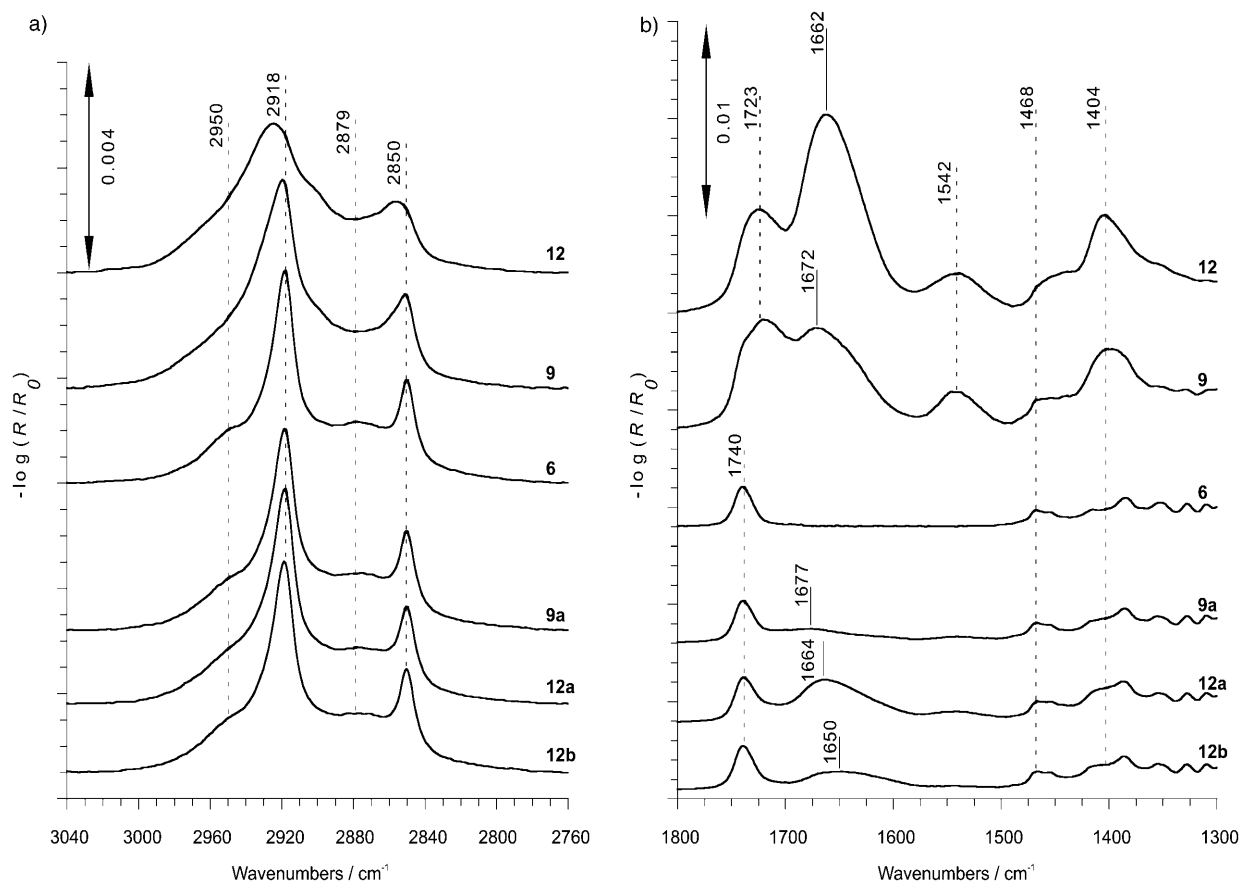
Figure 2. a) Infrared reflection–absorption spectra of one-component SAMs **6**, **9**, and **12** and mixed SAMs **9a**, **12a**, and **12b**, showing the CH stretching region (see Figure 1 or text for the description). b) The fingerprint region.

SAM **9a**, a significant deviation from the expected factor of 2. To reduce the amount of compound **12** in the mixed SAMs, we changed the solvent from acetonitrile to THF. This effect is confirmed by the reduced thickness values (Figure 1) for SAM **12b** as compared to SAM **12a** (≈ 2 Å difference) and by an increase in θ_a. Importantly, the IRAS data show that the change of solvent does not affect the structure of the alkyl layer (Figure 2a). A slight red shift of the $\nu_a(COO^-)$ mode (Figure 2b) can be explained by the presence of different counter-ions in the samples after drying. The peak integration procedure for SAM **12b** suggests that the total amount of the NTA moieties is now 1.5 times higher than in the case of SAM **9a**. We would like to stress, however, that the IR peak analysis yields only an approximate estimation of the amount of mono- and bis-NTA groups in the SAMs under investigation because of possible differences in peak intensity due to electrostatic interaction and/or orientation effects. Nevertheless, the employed set of surface analysis techniques clearly shows that SAMs **9a** and **12b** each consist of a highly ordered alkyl layer, which is in turn covered by an amorphous-like EG$_3$ layer with sparsely distributed mono- or bis-NTA moieties. The stoichiometric ratios of the constituent functional thiol molecules in these SAMs are very similar and each functional thiol molecule corresponds to one docking site for one His$_6$ tag. The well

defined SAMs **9a** and **12b** were therefore used for further investigation.

Protein immobilization proofing specificity, activity, and reversibility: As a model system with which to evaluate the developed sensor surface we chose the His$_6$-tagged extracellular domain of the human interferon receptor ifnar2 (His$_6$ ifnar2) and its ligand IFNα2. This protein has been shown to be highly sensitive to immobilization procedures,[50] and so is well suited for study of functional immobilization. Here, receptor immobilization and subsequent ligand binding was monitored in real-time by surface plasmon resonance.

First, protein immobilization on a bis-NTA chip surface (SAM **12b**) was monitored by injection of His$_6$ ifnar2 (300 nM). After monitoring of receptor association and dissociation, the chip surface was regenerated by use of imidazole (1 M) and EDTA (200 mM) and used again. Figure 3a shows three overlaid sensorgrams of repeated His$_6$ ifnar2 immobilization on an individual chip. The signal response, which is proportional to the amount of immobilized protein, remains almost constant at approximately 850 resonant units (RUs), demonstrating efficient regeneration and high reproducibility of protein immobilization on the chip surface. For the sake of simplicity the regeneration steps are omitted in the sensorgrams. Hence, the same chip can be reused for
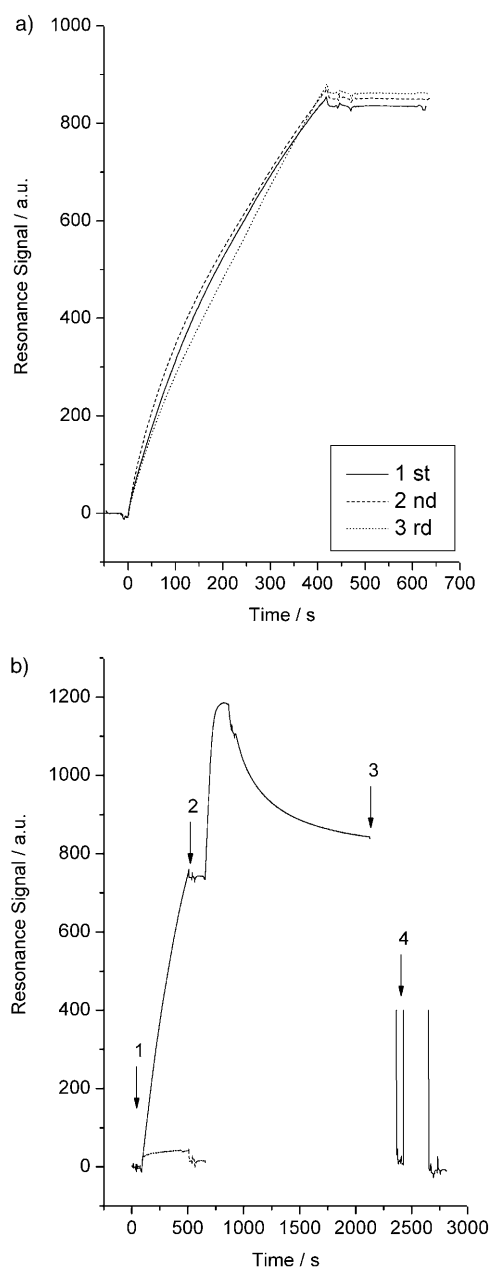
Figure 3. Specific receptor binding and ligand interaction followed by surface plasmon resonance. a) A bis-NTA chip was used for immobilization of His$_6$-tagged receptor His$_6$ ifnar2 and regenerated completely three times, demonstrating the high reproducibility of the protein immobilization. Regeneration of the chip surface was achieved by injection of imidazole and EDTA. The sensorgrams of the first, second, and third cycles of immobilization are overlaid; the regeneration steps are not shown. Resonance units (RUs) are plotted in arbitrary units (a.u.). b) Typical sensorgrams of immobilized His$_6$ ifnar2 and subsequent binding of its ligand IFNα2 on a functionalized multivalent bis-NTA surface with (solid) and without (dashed) loaded nickel ions. Injection of His$_6$ ifnar2 (1), followed by IFNα2 (2). After the binding experiment, the chip surface was regenerated with imidazole (3) and EDTA (4).

protein immobilization many times with the same binding capacity.

We next performed ligand–receptor interaction assays with His$_6$ ifnar2 and its ligand IFNα2 on multivalent chela-

tor SAMs. Figure 3b shows the sensorgram of receptor immobilization on a bis-NTA SAM. After activation of the bis-NTA chips with nickel ions, followed by washing with buffer, the injection of His$_6$ ifnar2 (300 nM) yielded a stable signal of approximately 750 RU (step 1). Subsequent binding of IFNα2 demonstrated that approximately 90% of immobilized His$_6$ ifnar2 remained functional (step 2). IFNα2 dissociates from His$_6$ ifnar2 with its typical dissociation rate constant of around 0.01 s^{-1}[50] and thus confirms the specificity of the interaction to the immobilized His$_6$-tagged receptor. After injection of imidazole (1 M) and EDTA (200 mM) (steps 3 and 4) immobilized His$_6$ ifnar2 is almost completely removed and the metal-chelating surface is recovered. In contrast to this specific binding assay, nonspecific binding of the receptor to the functionalized surface was negligibly low in the absence of nickel ions (ca. 40 RU; dashed line). In the absence of immobilized receptor under identical conditions, only 1% nonspecific binding of IFNα2 was observed (data not shown).

Both types of chelating SAMs, with mono-NTA thiols and also with bis-NTA thiols, show similar protein binding behavior with respect to specificity and functionality of the immobilized protein. The key difference between mono- and multivalent chelator SAMs becomes evident in imidazole competition assays. We systematically compared the effect of dissociation of His$_6$ ifnar2 from mono-NTA and bis-NTA SAMs at increasing imidazole concentrations (0–20 mM) (Figure 4a and b). The strongly decreased dissociation rate of the His$_6$-tagged protein from the bis-NTA group in relation to the conventional mono-NTA group is evident. Unlike the conventional mono-NTA, multivalent chelator chips exhibit a decreased dissociation rate of His$_6$ ifnar2 (Figure 4c). The desorption kinetics of His$_6$ ifnar2 from the mono- and multivalent chelator surface as a function of the imidazole concentration are compared in Figure 4d. A clear shift of the imidazole-induced complex dissociation to higher imidazole concentrations from mono-NTA to bis-NTA complexes was observed. The half-life of protein binding in the bis-NTA/His$_6$ tag complex was prolonged in relation to that in the mono-NTA/His$_6$ tag complex due to multivalent interactions. These different dissociation properties enable orthogonal protein immobilization with use of the same tag but various (mono- or multivalent) chelators. Furthermore, chip-to-chip variations are negligible, as demonstrated by the remarkably high reproducibility of the SPR experiments. The introduction of the bis-NTA unit enables quasi-irreversible, highly specific, and switchable immobilization of functional His$_6$-tagged proteins.

Patterned protein arrays on multivalent chelator SAMs: Since the multivalent chelator chip proved superior in terms of specificity, stability, and reversibility in the non-label detection (SPR) set-up, it would also be interesting to explore its compatibility by fluorescence techniques. In addition, the multivalent chelating surfaces arranged in the microarray format should be useful for protein chip applications. We therefore microfabricated a surface consisting of 100 μm ×
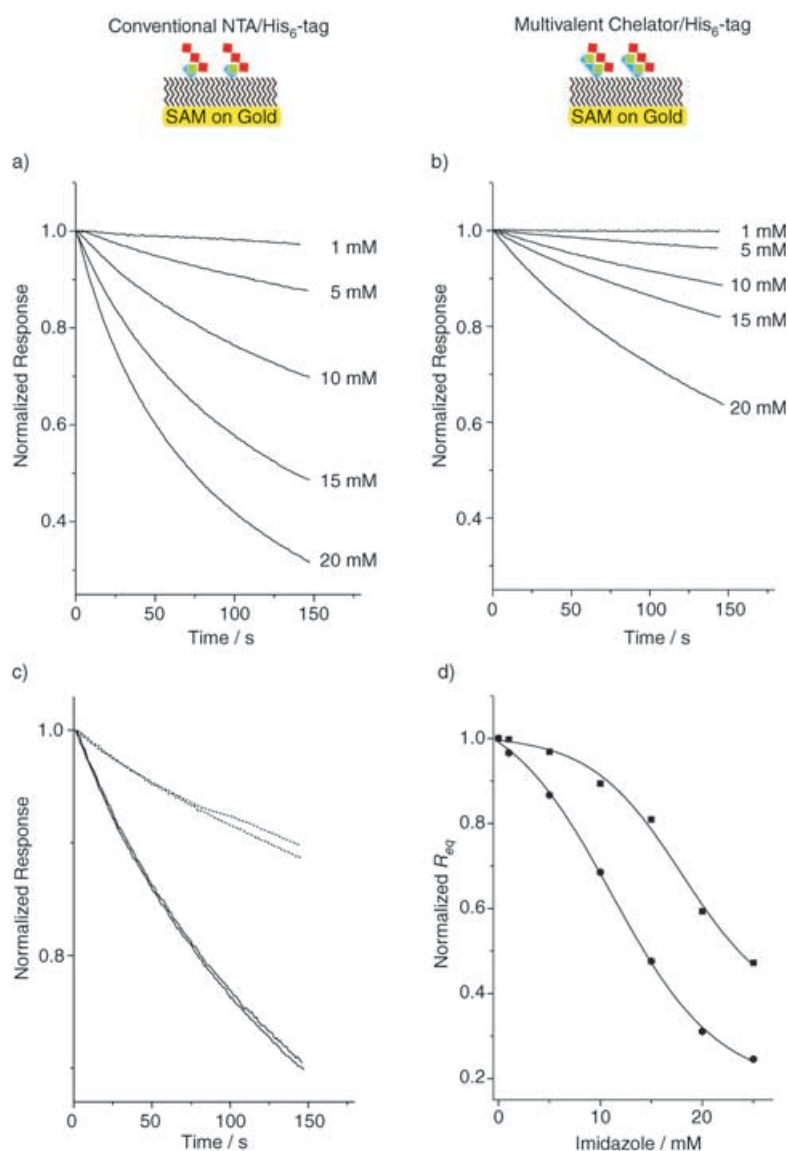
Figure 4. Different stabilities of the mono-NTA and bis-NTA chips. a) Increasing concentrations of imidazole induce dissociation of immobilized His₆ ifnar2 on the mono-NTA and b) on the bis-NTA surface with different rates. c) Imidazole (10 mM) affects dissociation of immobilized His₆ ifnar2 on two individual bis-NTA chip surfaces (dashed, upper) and two individual mono-NTA surfaces (solid, lower) with different efficiency. d) Bis-NTA/His₆ tag complexes dissociate only at higher imidazole concentrations. Bis-NTA SAMs (square) exhibit an increased stability of the complex in comparison to mono-NTA SAMs (circle). Imidazole-induced complex dissociation is shifted to higher concentrations.

power, enabled us to record fluorescence images by laser scanning microscopy (Figure 5). We observed that BSA efficiently blocks the imprinted hydrophobic grid (dark areas, Figure 5a). The Oregon Green-labeled, His₆-tagged maltose-binding protein (OG His₆ MBP) binds specifically only to the microarrays functionalized by multivalent chelator SAMs (green squares). An additional test of the selectivity of the patterned multivalent sensor surface can be performed by adsorbing Texas Red-labeled bovine serum albumin (TR-BSA) to the chip structured in the same way as before (Figure 5b). Two-color imaging confirms that the unspecific binding of TR-BSA to the pattern of bis-NTA SAM is extremely low and does not interfere with the binding of OG His₆ MBP. Such orthogonal protein microstructures remained on the chip surface for at least 24 h under buffer flow at room temperature (not shown). Moreover, as can be seen in Figure 5c and d, the chip could easily be regenerated by addition of imidazole. It is worth mentioning that the slight variation in fluorescence intensities is due to inhomogeneous laser illumination and to a certain spectral cross-talk between the employed fluorescent probes. The latter instrumental factor can be easily minimized when only one labeled protein is used (see Figure 5a). In summary, the high selectivity, stability, and reversibility of these multivalent NTA SAMs open the possibility to construct novel protein chip architectures for high-throughput screening of ligand–receptor and protein–protein interactions.

Uniform orientation of protein complexes monitored at single-molecule level: Observation of the chip surface at the molecular scale gives insights into the orientations and structures of immobilized proteins. AFM is the method of choice with which to investigate surface topography and properties at molecular scales. SAMs of multivalent chelator

100 μm functional areas of bis-NTA SAMs with passivated separations of 45 μm. First, microcontact printing was employed to generate a hydrophobic eicosane thiol SAM on gold, to form a grid separating the square-shaped areas, which were left available for subsequent filling with multivalent bis-NTA SAM **12b**. Such chips were activated with nickel ions, and were then sequentially exposed to fluorescence-labeled or nonlabeled proteins. In general, visualization of fluorescent species on gold surfaces is complicated because of strong fluorescence quenching.[51] However, the separation between the fluorescent probes and the gold surface by the bis-NTA SAM layer, together with a high laser
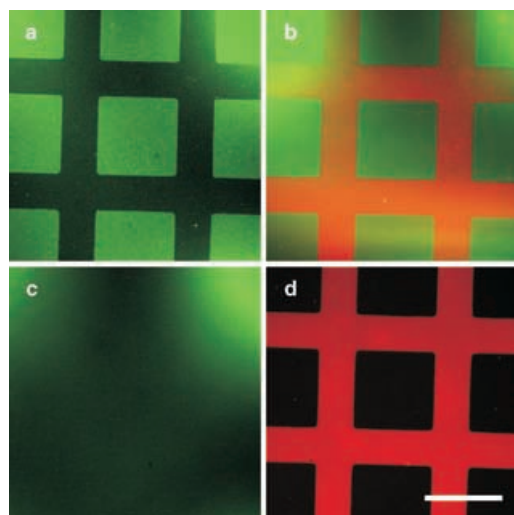
Figure 5. Laser scanning microscopy images of two patterned bis-NTA chips exposed to different fluorescent-labeled and nonlabeled proteins. a) Green fluorescence image of a chip loaded first with BSA and then with Oregon Green-labeled (OG-labeled) His$_6$ MBP. b) An overlay image of red and green fluorescence channels of another chip loaded first with Texas Red-labeled BSA and then with OG His$_6$-MBP. c) The same chip as in b), but recorded with green fluorescence channel after injection of imidazole. d) The same experiment as in c), red fluorescence channel. The scale bar is 100 μm. Details are given in Experimental Section.

thiols were prepared on ultra-flat, template-stripped gold (TSG) and studied during the process of protein immobilization. The model system for these AFM-based studies was the 20S proteasome from *Thermoplasma acidophilum*.[52] This barrel-shaped multicatalytic protease complex (700 kDa) is fundamental in protein degradation in the cytosol and therefore essential for many cellular processes.[53–55] Because of its molecular dimensions of 11×15 nm,[56] the proteasome is ideal for single-molecule studies by AFM. For specific binding to chelator SAMs, we used His$_6$-tagged proteasomes (βC-His$_6$ proteasome) enabling a well-defined and uniform immobilization in the "side-on" orientation. Previous studies using metal-chelating lipid layers have demonstrated absolute control of the orientation of immobilized proteasomes.[31,32] Figure 6a shows a representative topographic AFM image of a bis-NTA SAM formed on TSG before addition of protein. The image

was obtained in Tapping Mode under buffer and is largely featureless (RMS value ≈5 Å), which is due to the high quality of the ultraflat gold surface (RMS value ≈2 Å). After activation with nickel ions and immobilization of His$_6$-tagged proteasome, a homogenous distribution of proteasome molecules becomes visible (Figure 6b). After subsequent washing with imidazole and EDTA, the surface was largely recovered and only a few isolated traces of unspecific adsorbed proteins are visible (Figure 6c).

The AFM experiments demonstrate that immobilization is uniform even at a single-molecule level. The height of the immobilized molecules determined by image analyses amounts to 10–11 nm, which is in accordance with the diameter of the 20S proteasome (11 nm).[56] A very straightforward method to determine the height of the immobilized protein monolayer, and hence the molecular orientation, is local nano-shaving of the proteins, which yields a value of 10–11 nm. The corresponding data and experimental description are presented in the Supporting Information (see Figure S1). The lateral dimensions, however, are 15–20 nm. This value, slightly larger than the proteasome's dimension (15 nm), can be explained by the tip-broadening effect in AFM.[57] Because of the location of the His$_6$-tag, immobilized proteasome molecules are entirely oriented in this "side-on" orientation, as can be seen in Figure 6d/e. Barrel-shaped or oval molecules are visible at scans of 415×415 nm (Figure 6d). The homogenous orientation and distribution of immobilized protein complexes on this chelating surface allows almost absolute control over the orientation and function of the protein and thus represents an optimal plat-
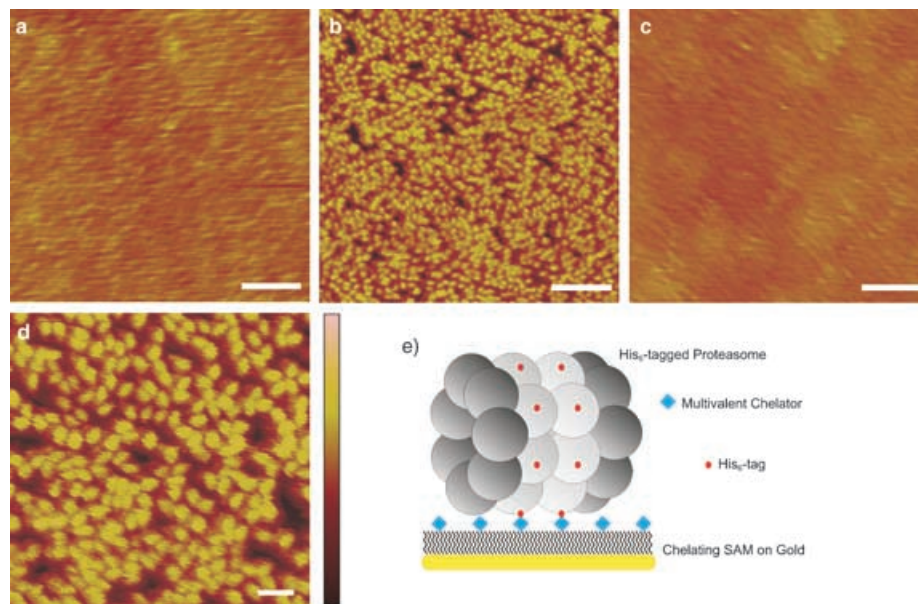

Figure 6. AFM study of protein immobilization on chelating SAMs. a) SAM of bis-NTA thiol on template-stripped gold before and b) after immobilization of βC-His$_6$ proteasomes, and c) after regeneration with imidazole and EDTA. The scan size was always 1 μm and the scale bar is 0.2 μm. d) In this 415 nm AFM scan the so-called "side-on" orientation of the proteasome is obvious. The scale bar is 50 nm. e) The cartoon illustrates the sites of the His$_6$-tags on this proteasome variant and the orientation of the proteasome in the immobilized state on the multivalent chelating SAM. The *z*-data scale in all AFM images represents the height from 0 to 15 nm.

form for single-molecule studies, force spectroscopy experiments, and quantitative protein–protein interaction studies in which control of ligand-binding site is desirable. High-density packing of immobilized proteins allows tailoring of protein chip architectures in nano-dimensions.

Conclusion

The conventional NTA/His$_6$ tag technique has been successfully extended to self-assembling, multivalent chelator thiols both for high-affinity recognition and for stable and uniform immobilization of His$_6$-tagged proteins on chip surfaces. Bis-NTA was linked through an oligoethylene glycol to alkyl thiols by an efficient modular synthesis strategy to yield a novel, multivalent compound for formation of mixed SAMs on gold. These multivalent chelator chips allow specific, high-affinity, reversible, long-term immobilization of His$_6$-tagged proteins. SPR experiments with receptors successfully demonstrated the suitability of this format for delicate biophysical assays with high reproducibility. Microstructured chip surfaces allow the generation of protein microarrays for high-throughput screening by fluorescence techniques. In AFM studies the reversibility of the specific protein immobilization process was visualized at single-molecule levels. The total control over the orientation of the immobilized protein promotes this chip surface as an optimal platform for studies focusing on research targets at single-molecule levels and for nanobiotechnology. The homogeneous orientation and distribution of immobilized proteins demonstrate the high quality of the designed surface and qualify its application in nano-scaled protein chip architectures.

Experimental Section

Materials: The synthesis of the chelators and thiol compounds is described in detail in the Supporting Information. All solvents were p. a. purity grade. TLC was performed on Merck 60 F-254 layers, and results were viewed by use of UV light and/or AMC reagent (5 g ammonium molybdate and 1 g cerium sulfate in 1 L 10% H$_2$SO$_4$) followed by heating, or with iodine vapor. Amines were stained by ninhydrin (0.3% in ethanol). Column chromatography was performed on silica gel (Merck). Solvents were evaporated on a rotary evaporator under reduced pressure and temperatures <50°C. NMR spectra were recorded on a Bruker spectrometer in CDCl$_3$ (Aldrich) as solvent and with TMS (0.05%, δ = 0.00 ppm) as internal standard. Proteins were produced and purified according to the given references in the methods section or were obtained commercially.

Preparation of gold surfaces: Gold surfaces were prepared by evaporation of thin gold films on standard (100)-silicon wafers, glass, or mica (muscovite mica V-1 or V-2). Wafer and glass substrates were cleaned before and after evaporation in a 5:1:1 mixture of MilliQ water, hydrogen peroxide (25%), and ammonia (30%) for 5 minutes at 85°C, followed by rinsing in MilliQ water. Wafer substrates were prepared as published previously[42] and used for contact angle goniometry, ellipsometry, infrared reflection–absorption spectroscopy, and fluorescence microscopy. To perform surface plasmon resonance experiments glass substrates were coated with a 2.5 nm layer of chromium followed by deposition of a 40 nm thick gold layer in a Bal-Tec Med020 system (Bal-Tec AG, Liechtenstein). For atomic force microscopy, mica substrates were prepared by

the template-stripped gold protocol as previously described.[58] Mixed SAMs were formed from solutions of matrix thiol and either mono-NTA thiol or bis-NTA thiol (20 μM final concentration in acetonitrile or THF). After chemisorption (for 24 h), the SAMs were sonified in acetonitrile or THF and in MilliQ water, and were stored in MilliQ water if not immediately used.

Contact angle goniometry: Contact angles were measured with a Ramé-Hart NRL 100 goniometer (Ramé-Hart, Mountain Lakes, USA) without control of the humidity in the ambient, with use of MilliQ water. Taking the high surface energy of the hydrophilic surfaces into account, only one measurement of the advancing and the receding contact angle was performed per sample.

Ellipsometry: For single-wavelength ellipsometry (AutoEL, Rudolph Research, Flanders, USA), average values of the refractive index of the clean gold sample, analyzed prior to the incubation, were used. The refractive index of the substrate and the results of the ellipsometric measurements on the SAMs were taken into an "ambient/organic film/gold" model, with the assumption of an isotropic, transparent organic film[59] with a refractive index of $n = 1.5$.[43,60,61] The film thickness was calculated as an average at three different spots on at least four samples for each SAM.

Infrared reflection-absorption spectroscopy (IRAS): The reflection-absorption spectra were recorded at room temperature on a Bruker IFS 66 system (Bruker Optik GmbH, Bremen, Germany), equipped with a grazing angle (85°) infrared reflection accessory and a liquid nitrogen-cooled MCT detector. The measurement chamber was continuously purged with nitrogen gas during the measurements. The acquisition time was around 10 minutes at 2 cm^{-1} resolution, and a three-term Blackmann–Harris apodization function was applied to the interferograms before Fourier transformation. SAMs of deuterated hexadecane thiolate (HS-(CD$_2$)$_{15}$CD$_3$) were used as reference.

Surface plasmon resonance (SPR): SAM surfaces were prepared in solutions of matrix thiol **6** (97 mol%) and either mono-NTA **9** or bis-NTA thiol **12** (3 mol%). SPR measurements were performed on a BIAcore X system (BIAcore AB, Uppsala, Sweden) at 25°C, with a flow rate of 10 μL min^{-1}, if not stated otherwise. HBS buffer (10 mM HEPES, 150 mM NaCl, pH 7.5) was used as running buffer and for all dilutions. Protein immobilization on the chelating SAM surface was carried out by sequential injections of NiSO$_4$ (100 mM, 35 μL), followed by injection of HBS buffer supplemented with imidazole (200 mM, 35 μL), and then followed by addition of His$_6$-tagged interferon receptor (His$_6$ ifnar2, 300 nM).[62] To study the activity of His$_6$ ifnar2 after immobilization, its ligand IFNα2 (200 nM, 35 μL)[62] was injected. To determine the amount of unspecific binding, the immobilization protocol was carried out identically, but without addition of nickel ions. In imidazole competition experiments, increasing concentrations of imidazole were injected after specific immobilization of His$_6$ ifnar2 at flow rates of 40 μL min^{-1}. The surface was rinsed with HBS buffer after each injection. Imidazole (1 M) and EDTA (200 mM) diluted in HBS buffer were used to remove the protein and the Ni^{2+} ions, respectively. Data evaluation was performed with standard analysis software. The equilibrium surface loading R_{eq} was normalized to the initial surface loading R_0.

Microcontact-printed bis-NTA chips: The PDMS stamps were prepared on the same master as described by Zhou et al., and under similar conditions.[63] For microcontact printing (μCP) we used the general protocol developed by Delamarche and co-workers.[64] Briefly, the prepolymer was cured in an oven at 65°C for around 2 h. Before the imprinting, the stamps were rinsed with ethanol, blown dry with nitrogen gas, and inked by application of a droplet (1 μL μm^{-2} area of the stamp) of ethanolic solution of eicosane thiol (200 μM) for 30 s. The excess liquid was blown away from a stamp with the nitrogen gas and the stamp was further dried under stream for another 30 s. The stamp was then immediately brought into contact with a gold chip for 3–10 s. Afterwards the chip was soaked in a 20 μM solution of **6** (97 mol%) and **12** (3 mol%) in acetonitrile. The adsorption time ranged from 3 to 48 h. The prepared chips were washed and loaded with Ni^{2+} ions as described above.

Fluorescence microscopy: The binding of the fluorescent proteins to the patterned bis-NTA chips was followed by confocal laser scanning micro-

scopy (LSM 510, Carl Zeiss, Jena, Germany). Firstly, the chip was placed in a disposable Petri dish and incubated with either unlabeled or Texas Red-labeled (TR-labeled) bovine serum albumin (100 µg mL⁻¹ protein; Molecular Probes) for 10 min. After protein adsorption, the chip was thoroughly rinsed with the buffer, such that the surface remained wet all the time. Subsequently, the chip was exposed for 10 min to a mixed solution of unlabeled (2.5 µM) or Oregon Green-labeled (OG-labeled; 125 nM) His₆-tagged maltose-binding protein. His₆-tagged maltose-binding protein was purified by the standard IMAC procedure. After rinsing, the wet chips were immediately mounted into a custom-built flow chamber and were imaged by use of a Plan-Neofluor 40× oil-immersion objective (NA 1.3) and an inverted microscope setup (Axiovert 200M, Carl Zeiss, Jena, Germany). Argon (488 nm, 25 mW) and HeNe (543 nm, 1 mW) lasers were used for the excitation of Oregon Green and Texas Red, respectively. The image size was 2048×2048 pixels, corresponding to an area of 326×326 µm.

Atomic force microscopy (AFM): AFM experiments were performed with a Digital Instruments NanoScope IIIa SPM MultiMode atomic force microscope (Veeco Instruments, Santa Barbara, CA) in a commercial quartz fluid cell. NP-S cantilevers with a force constant of 0.06 N m⁻¹ (Veeco Instruments) were used for all experiments. Imaging was performed in tapping mode at resonance frequencies of around 9 kHz in HBS buffer and at drive amplitudes of 100 to 150 mV. All solutions were prepared or diluted in HBS buffer. The chelating SAMs were activated with NiSO₄ solution (5 mM) for 20 min, rinsed with HBS buffer, and incubated for 30 min at 4°C with βC-His₆-tagged proteasomes (30 nM).[32,52] Specifically immobilized proteins were detached in HBS buffer supplemented with imidazole (1 M) and EDTA (500 mM). Imaging of the surface was always performed in HBS buffer between these steps.

Acknowledgements

[1] M. P. Washburn, *Nat. Biotechnol.* **2003**, *21*, 1156–1157.
[2] D. S. Wilson, S. Nock, *Curr. Opin. Chem. Biol.* **2002**, *6*, 81–85.
[3] G. MacBeath, *Nat. Genet.* **2002**, *32*, 526–532.
[4] S. Y. Seong, C. Y. Choi, *Proteomics* **2003**, *3*, 2176–2189.
[5] P. F. Predki, *Curr. Opin. Chem. Biol.* **2004**, *8*, 8–13.
[6] J. LaBaer, N. Ramachandran, *Curr. Opin. Chem. Biol.* **2005**, *9*, 14–19.
[7] H. Zhu, M. Snyder, *Curr. Opin. Chem. Biol.* **2003**, *7*, 55–63.
[8] H. Zhu, M. Bilgin, R. Bangham, D. Hall, A. Casamayor, P. Bertone, N. Lan, R. Jansen, S. Bidlingmaier, T. Houfek, T. Mitchell, P. Miller, R. A. Dean, M. Gerstein, M. Snyder, *Science* **2001**, *293*, 2101–2105.
[9] P. D. Gershon, S. Khilko, *J. Immunol. Methods* **1995**, *183*, 65–76.
[10] S. Quetglas, C. Leveque, R. Miquelis, K. Sato, M. Seagar, *Proc. Natl. Acad. Sci. USA* **2000**, *97*, 9695–9700.
[11] I. Gokce, E. M. Raggett, Q. Hong, R. Virden, A. Cooper, J. H. Lakey, *J. Mol. Biol.* **2000**, *304*, 621–632.
[12] M. R. Martzen, S. M. McCraith, S. L. Spinelli, F. M. Torres, S. Fields, E. J. Grayhack, E. M. Phizicky, *Science* **1999**, *286*, 1153–1155.
[13] H. Bach, Y. Mazor, S. Shaky, A. Shoham-Lev, Y. Berdichevsky, D. L. Gutnick, I. Benhar, *J. Mol. Biol.* **2001**, *312*, 79–93.
[14] P. Riggs, *Mol. Biotechnol.* **2000**, *15*, 51–63.
[15] B. A. Bouchard, B. Furie, B. C. Furie, *Biochemistry* **1999**, *38*, 9517–9523.

[16] D. L. Pearson, R. D. Reimonenq, K. M. Pollard, *Protein Expression Purif.* **1999**, *17*, 49–56.
[17] J. Schmitt, H. Hess, H. G. Stunnenberg, *Mol. Biol. Rep.* **1993**, *18*, 223–230.
[18] J. A. Bornhorst, J. J. Falke, *Methods Enzymol.* **2000**, *326*, 245–254.
[19] E. Hochuli, *J. Chromatogr.* **1988**, *444*, 293–302.
[20] E. Hochuli, *Genet. Eng.* **1990**, *12*, 87–98.
[21] M. Kindermann, N. George, N. Johnsson, K. Johnsson, *J. Am. Chem. Soc.* **2003**, *125*, 7810–7811.
[22] Y. Kwon, Z. Han, E. Karatan, M. Mrksich, B. K. Kay, *Anal. Chem.* **2004**, *76*, 5713–5720.
[23] C. D. Hodneland, Y. S. Lee, D. H. Min, M. Mrksich, *Proc. Natl. Acad. Sci. USA* **2002**, *99*, 5048–5052.
[24] F. H. Arnold, *Metal-affinity protein separations*, Academic Press, San Diego, **1992**.
[25] E. Hochuli, W. Bannwarth, H. Döbeli, R. Gentz, D. Stüber, *Bio-Techniques* **1988**, *6*, 1321–1325.
[26] I. T. Dorn, K. R. Neumaier, R. Tampé, *J. Am. Chem. Soc.* **1998**, *120*, 2753–2763.
[27] L. Nieba, S. E. Nieba-Axmann, A. Persson, M. Hamalainen, F. Edebratt, A. Hansson, J. Lidholm, K. Magnusson, A. F. Karlsson, A. Plückthun, *Anal. Biochem.* **1997**, *252*, 217–228.
[28] L. Schmitt, C. Dietrich, R. Tampé, *J. Am. Chem. Soc.* **1994**, *116*, 8485–8491.
[29] D. R. Shnek, D. W. Pack, D. Y. Sasaki, F. H. Arnold, *Langmuir* **1994**, *10*, 2382–2388.
[30] I. T. Dorn, K. Pawlitschko, S. C. Pettinger, R. Tampé, *Biol. Chem.* **1998**, *379*, 1151–1159.
[31] I. T. Dorn, R. Eschrich, E. Seemüller, R. Guckenberger, R. Tampé, *J. Mol. Biol.* **1999**, *288*, 1027–1036.
[32] A. Thess, S. Hutschenreiter, M. Hofmann, R. Tampé, W. Baumeister, R. Guckenberger, *J. Biol. Chem.* **2002**, *277*, 36321–36328.
[33] A. Ulman, *Chem. Rev.* **1996**, *96*, 1533–1554.
[34] C. Pale-Grosdemange, E. S. Simon, K. L. Prime, G. M. Whitesides, *J. Am. Chem. Soc.* **1991**, *113*, 12–20.
[35] G. B. Sigal, C. Bamdad, A. Barberis, J. Strominger, G. M. Whitesides, *Anal. Chem.* **1996**, *68*, 490–497.
[36] L. Schmitt, M. Ludwig, H. E. Gaub, R. Tampé, *Biophys. J.* **2000**, *78*, 3275–3285.
[37] M. Mrksich, C. S. Chen, Y. N. Xia, L. E. Dike, D. E. Ingber, G. M. Whitesides, *Proc. Natl. Acad. Sci. USA* **1996**, *93*, 10775–10778.
[38] K. L. Prime, G. M. Whitesides, *Science* **1991**, *252*, 1164–1167.
[39] D. K. Schwartz, *Annu. Rev. Phys. Chem.* **2001**, *52*, 107–137.
[40] R. Valiokas, S. Svedhem, M. Ostblom, S. C. T. Svensson, B. Liedberg, *J. Phys. Chem. B* **2001**, *105*, 5459–5469.
[41] P. Harder, M. Grunze, R. Dahint, G. M. Whitesides, P. E. Laibinis, *J. Phys. Chem. B* **1998**, *102*, 426–436.
[42] R. Valiokas, S. Svedhem, S. C. T. Svensson, B. Liedberg, *Langmuir* **1999**, *15*, 3390–3394.
[43] C. D. Bain, E. B. Troughton, Y. T. Tao, J. Evall, G. M. Whitesides, R. G. Nuzzo, *J. Am. Chem. Soc.* **1989**, *111*, 321–335.
[44] R. Valiokas, M. Ostblom, S. Svedhem, S. C. T. Svensson, B. Liedberg, *J. Phys. Chem. B* **2002**, *106*, 10401–10409.
[45] L. Malysheva, Y. Klymenko, A. Onipko, R. Valiokas, B. Liedberg, *Chem. Phys. Lett.* **2003**, *370*, 451–459.
[46] R. G. Nuzzo, L. H. Dubois, D. L. Allara, *J. Am. Chem. Soc.* **1990**, *112*, 558–569.
[47] M. Liley, T. A. Keller, C. Duschl, H. Vogel, *Langmuir* **1997**, *13*, 4190–4192.
[48] J. K. Lee, Y. G. Kim, Y. S. Chi, W. S. Yun, I. S. Choi, *J. Phys. Chem. B* **2004**, *108*, 7665–7673.
[49] R. Arnold, W. Azzam, A. Terfort, C. Woll, *Langmuir* **2002**, *18*, 3980–3992.
[50] J. Piehler, G. Schreiber, *Anal. Biochem.* **2001**, *289*, 173–186.
[51] D. H. Waldeck, A. P. Alivisatos, C. B. Harris, *Surf. Sci.* **1985**, *158*, 103–125.
[52] E. Seemüller, A. Lupas, D. Stock, J. Löwe, R. Huber, W. Baumeister, *Science* **1995**, *268*, 579–582.

[53] D. Voges, P. Zwickl, W. Baumeister, *Annu. Rev. Biochem.* **1999**, *68*, 1015 – 1068.

[54] P. Zwickl, D. Voges, W. Baumeister, *Philos. Trans. R. Soc. London Ser. B* **1999**, *354*, 1501 – 1511.

[55] M. Bochtler, L. Ditzel, M. Groll, C. Hartmann, R. Huber, *Annu. Rev. Anthropol. Annu. Rev. Bioph. Biom.* **1999**, *28*, 295 – 317.

[56] J. Löwe, D. Stock, B. Jap, P. Zwickl, W. Baumeister, R. Huber, *Science* **1995**, *268*, 533 – 539.

[57] M. J. Allen, N. V. Hud, M. Balooch, R. J. Tench, W. J. Siekhaus, R. Balhorn, *Ultramicroscopy* **1992**, *42–44*, 1095 – 1100.

[58] M. Hegner, P. Wagner, G. Semenza, *Surf. Sci.* **1993**, *291*, 39 – 46.

[59] D. L. Allara, R. G. Nuzzo, *Langmuir* **1985**, *1*, 45 – 52.

[60] M. D. Porter, T. B. Bright, D. L. Allara, C. E. D. Chidsey, *J. Am. Chem. Soc.* **1987**, *109*, 3559 – 3568.

[61] J. Shi, B. Hong, A. N. Parikh, R. W. Collins, D. L. Allara, *Chem. Phys. Lett.* **1995**, *246*, 90 – 94.

[62] J. Piehler, G. Schreiber, *J. Mol. Biol.* **1999**, *289*, 57 – 67.

[63] Y. Zhou, R. Valiokas, B. Liedberg, *Langmuir* **2004**, *20*, 6206 – 6215.

[64] E. Delamarche, H. Schmid, A. Bietsch, N. B. Larsen, H. Rothuizen, B. Michel, H. Biebuyck, *J. Phys. Chem. B* **1998**, *102*, 3324 – 3334.